Recoverable Energy in Photovoltaic Systems with Submodule Level Dispersion Losses ☆

Carlos Olalla*, Md. Nazmul Hasan, Luis Martínez-Salamero

Departament d'Enginyeria Elèctrica, Electrònica i Automàtica
Universitat Rovira i Virgili, Tarragona, 43007 Spain
(e-mail: carlos.olalla@urv.cat).

Abstract

Photovoltaic (PV) ageing is known to cause a linear degradation of the short-circuit and maximum power point currents, which results in the corresponding power loss. Nonetheless, besides of degradation, also a dispersion of these currents has been reported in the past. Such a dispersion induces significant mismatches in the PV system, even in the absence of partial shading, further increasing the power loss. Such a phenomenon has attracted the interest of investigators, as the fraction of power loss due to mismatch is recoverable. Nonetheless, all previous works have considered module-level ageing data, whereas the recoverable power at the submodule level may be larger. This paper investigates the effects of ageing at the submodule level, and compares the results with previously reported data. It is shown that previous works have underestimated the amount of recoverable power, and that the lifetime improvement of the energy yield may add up to 4 - 6% of the total.

Keywords: Photovoltaics, Submodule, Ageing, Degradation, Mismatch, Distributed MPPT, LCOE.

☆Published in Solar Energy
https://doi.org/10.1016/j.solener.2020.01.036
Received 18 October 2018; Received in revised form 30 October 2019; Accepted 13 January 2020
*Corresponding author

1. Introduction

Two main factors affect photovoltaic (PV) module long-term performance: degradation and mismatches. In order to be cost-efficient, PV modules must exhibit low levels of degradation. As an example, a linear degradation below 1% per year is one of the key factors that has been reported in studies on the levelized cost of photovoltaic energy (Jordan et al., 2016). This has motivated numerous studies on the experimental measurement of photovoltaic degradation rates (Vázquez and Rey-Stolle, 2008; Chamberlin et al., 2011; Jordan and Kurtz, 2011; Polverini et al., 2013; Makrides et al., 2014) and also on the study of degradation agents (Pozza and Sample, 2016; Gagliardi et al., 2017; Borri et al., 2018; Gagliardi and Paggi, 2018, 2019). With sample sizes from hundreds to only a few tens of measurements, numerous papers have reported that the median degradation rate for Mono and Poly-Si modules lies within the 0.5-0.6%/year range, whereas the mean degradation is slightly above, in the 0.8-0.9%/year range (Jordan et al., 2016). Populations are typically considered normal (gaussian) in these papers, although most of the previously mentioned references show some level of negative skewness in current and power (Jordan et al., 2012). In addition, the degradation is usually assumed to be linear, with the exception of some reports pointing to a higher beginning-of-life decline of the output power, specially in thin-film modules (Mikofski et al., 2012).

The second characteristic affecting the long-term performance of PV systems is the dispersion of relevant parameters, such as the maximum power voltage (V_{mp}) and current (I_{mp}). This dispersion induces mismatches when PV modules are connected in series, reducing the overall performance of the system. It is worth to note that such a loss only occurs due to the inability of the individual modules to operate at their respective maximum power points (MPP), so that it can be recovered with distributed power electronic converters (Olalla et al., 2015). As with the degradation rates, these mismatches have been analysed using normal models, extracted from measurements at the module level. However, less research has been focused on this point, and only a few results have been reported (Vázquez and Rey-Stolle, 2008; Chamberlin et al., 2011; Jordan et al., 2012). In these papers, the coefficient of variation (CV) of the short-circuit current has been shown to increase with time, from 1% in year 1 to 10% in year 25 (0.36% per year). The impact of this source of mismatch at the module level has been shown to be significant. In (Olalla et al., 2015), it was shown that the 25 years energy yield penalty is in the range of 2.5-3.0% of the total lifetime energy, with average power losses above 7% in the 25th year. Nonetheless, these predictions may be conservative. First, predictions have used the CV of the short-circuit current, whereas the modules operate at the maximum power point. Secondly, module-level measurements consider the series connection of a large number of cells. The effect of under-performing cells is, to some extent, compensated by the cells within the same module. In consequence, submodule-level CV may be higher than what has been reported at the module level, which would result in larger recoverable power losses.

This paper focuses on the measurement and the modeling of submodule-level ageing effects. The paper reports measurements in a population of 42 submodules, with emphasis on the differences with respect to previously reported module level measurements. Although the degradation rate should remain unaffected by the granularity level, it is expected that submodule level models will exhibit a higher coefficient of variation with respect to the module level. Attention is paid to differences between short-circuit and MPP currents, as the number of results showing both measurements is scarce.

Since there is potential for unmeasured energy yield penalty due to submodule-level mismatch, the paper also aims to quantify the recoverable power loss. First, the paper evaluates the skewness of the distributions and explores non-gaussian statistical models in PV parameter modeling. Although the use of non-gaussian models is not new (Pulver et al., 2010), this paper is the first that uses them to model MPP current dispersion at the submodule level. Also, it is shown that previously reported negative skewness in the power and current distributions of PV systems impacts on long-term forecasts. Then, the efficiency

and the 25 years energy yield of several PV systems is assessed by means of Monte Carlo simulations and compared with the previous results mentioned above.

2. Description of the Measurement Procedure and the Data Processing Method

The array under test consists of 14 Trina Solar modules TSM-PC05 230, each of which is composed of 3 submodules of 20 cells in series. The modules feature poly-Si standard screen-printed cells with a conventional screen-printed back-side. The modules are located in Tarragona (41.1189° N, 1.2445° E), they face due south and are tilted at 15 degrees from the horizontal (see Fig. 1(a)). The array is divided in two strings of 7 modules, connected to the grid through 2 StecaGrid 2000+ inverters. The modules, whose characteristics can be observed in Table 1, were installed in May 2010. All junction boxes were modified with additional connectors, in order to provide easy access to the individual submodules, which results in 42 submodule measurements.

Measurements were taken in the field, within 1 h of solar noon, under clear sky conditions and with irradiances above 800 W/m^2. Modules were cleaned 1 h before the measurements in order to remove dirt. A first class pyranometer (Hukseflux TR-11) in the plane of each PV module was used to obtain irradiance measurements. Temperature, voltage and current of the submodule under test were measured according to the IEC-60904 standard (IEC, 2006, 2011), with tolerances below 0.5°C for temperatures and below 0.15% for voltages and currents. Two consecutive I-V curves were taken for each submodule, and each I-V scan was completed in approximately 1.5 s, using the datalogging capabilities of a N4L PPA 1530 analyzer. Fig. 1(b) shows a block diagram of the set-up, where additional details of the different instruments can be observed.

Data were processed as follows. First, the data captured by the instruments were averaged to improve the basic accuracy of our setup. Every data point in the V-I curve is the result of averaging 3 consecutive measurements in the same point of the V-I sweep. These measurements in the same point are obtained every 2 ms. Typically, the two consecutive V-I curves obtained did not show significant differences, and only one was kept. Nonetheless, these replicas were useful in case of unaccounted changes in the environmental conditions (such as irradiance variations). Then, the data were adapted to 1000 W/m^2 and 45°C (NOCT), following the methods reported in Zoellick (Zoellick, 1990), Reis and Coleman (Reis et al., 2002), which in our set of measurements provided negligible differences (below the error tolerances) with respect to the methods in the IEC standard (IEC, 2009). In order to assess the quality of the measurements, the agreement between the two consecutive measurements was verified and irradiance changes during the measurements were checked to be below 1 W/m^2.

3. Submodule Level Mismatch

This section shows the results of our submodule level measurements and compares them with previously reported results at the module level. Three sets of measurements are shown. The first measurement was carried out in March 2017, when the PV modules were 7 years old. The second measurement was performed

Table 1: Electrical Data @ STC (TSM-230 PC/PA05)

Peak Power (P_{mp})	76.67 W (±3%)
Maximum Power Voltage (V_{mp})	9.73 V
Maximum Power Current (I_{mp})	7.90 A
Open Circuit Voltage (V_{oc})	12.37 V
Short Circuit Current (I_{sc})	8.53 A

(a) Picture of one of the modules in the array.

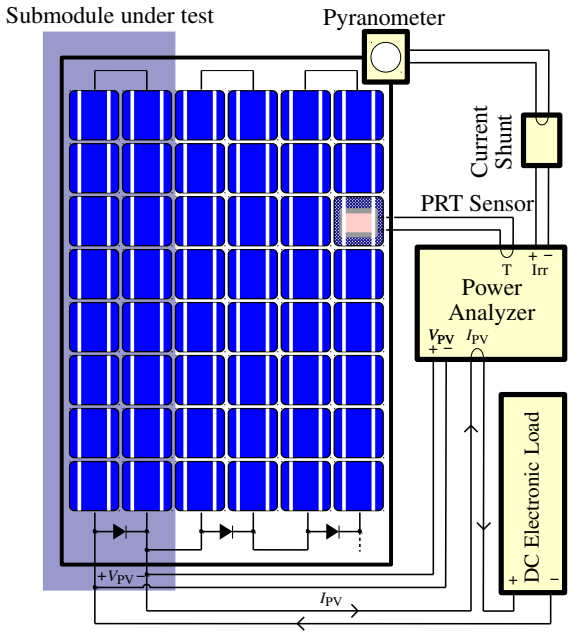

(b) Block diagram of the measurement setup. PV Module Trina TSM-PC05 230. Pyranometer Hukseflux TR-11. Temperature sensor: class A platinum resistance thermometer. DC Load BK Precision 8512. Power Analyzer and Logging: N4L PPA 1530.

Figure 1: Details on the array under test and the measurement setup.

one year later, in March 2018. The last measurement was carried out when the system was 9 years old, in March 2019.

3.1. Measurement Results

Figure 2 shows the normalized (NOCT) V-I curves of the measured 42 submodules, in 2017 (Fig. 2(a)) and 2019 (Fig. 2(b)). The data adapted to NOCT have been used to extract the short circuit current (I_{sc}), the open circuit voltage (V_{oc}), and the maximum power current, voltage and power (I_{mp}, V_{mp} and P_{mp}). As expected, it can be seen that the voltage parameters V_{oc} and V_{mp} exhibit smaller standard deviation and CV with respect to the current parameters I_{sc} and I_{mp}. In consequence, the CV of P_{mp} is in good agreement with that of I_{mp}. In addition, the histograms in the figures show negligible differences between the average and the median V_{mp}, whereas there is some level of discrepancy between the average and the median values of I_{sc} and I_{mp}. This also agrees with the previously mentioned skewness of these parameters.

Table 2 shows a summary of the statistical results for every parameter, considering the set of 42 submodule V-I curves: the average μ, the degradation of the average per year, the coefficient of variation and its change per year. No data of the first year of use is available, thus datasheet values are taken as a reference. It can be clearly seen how the current parameters I_{sc} and I_{mp} present large degradation rates around 1%, whereas the V_{oc} and V_{mp} remain mostly unaltered with time. After 9 years, the mean degradation rate of I_{sc} is -0.89%/year and that of I_{mp} is slightly above and equal to -1.02%. These values are in accordance with reported degradation rates of poly-Si modules (Jordan et al., 2012).

A more significant result with respect to mismatch due to ageing can be observed in the CVs of the table. First, the mismatch observed in I_{sc} and I_{mp} is significantly larger than that of V_{oc} and V_{mp}, in line

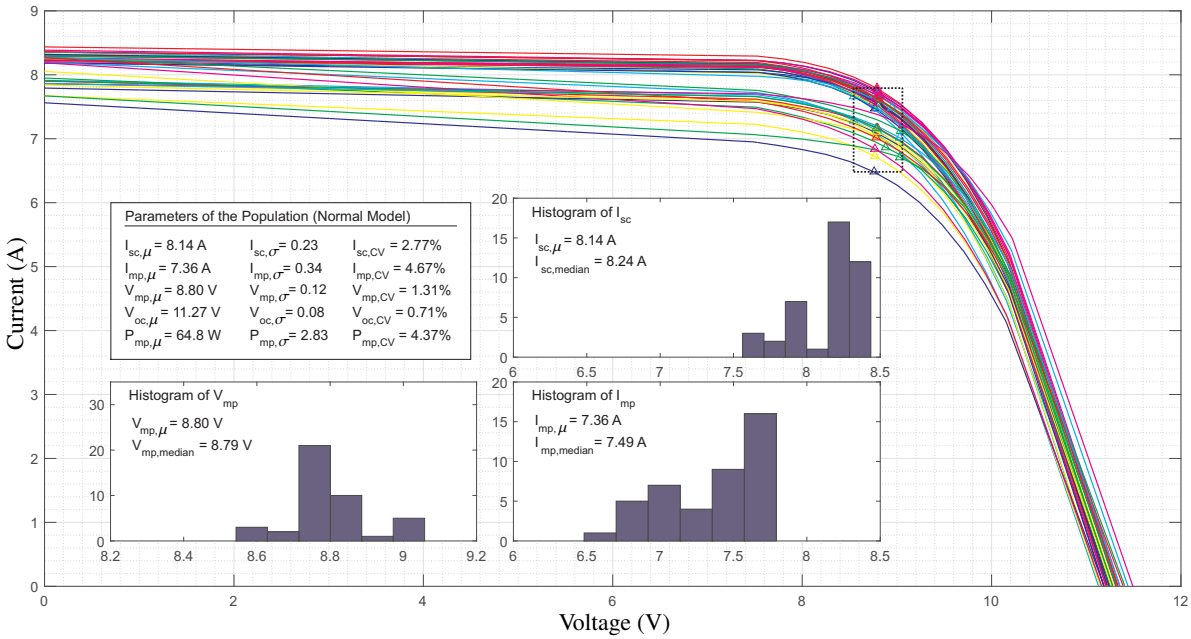

(a) Measurements in March 2017 (7 years old).

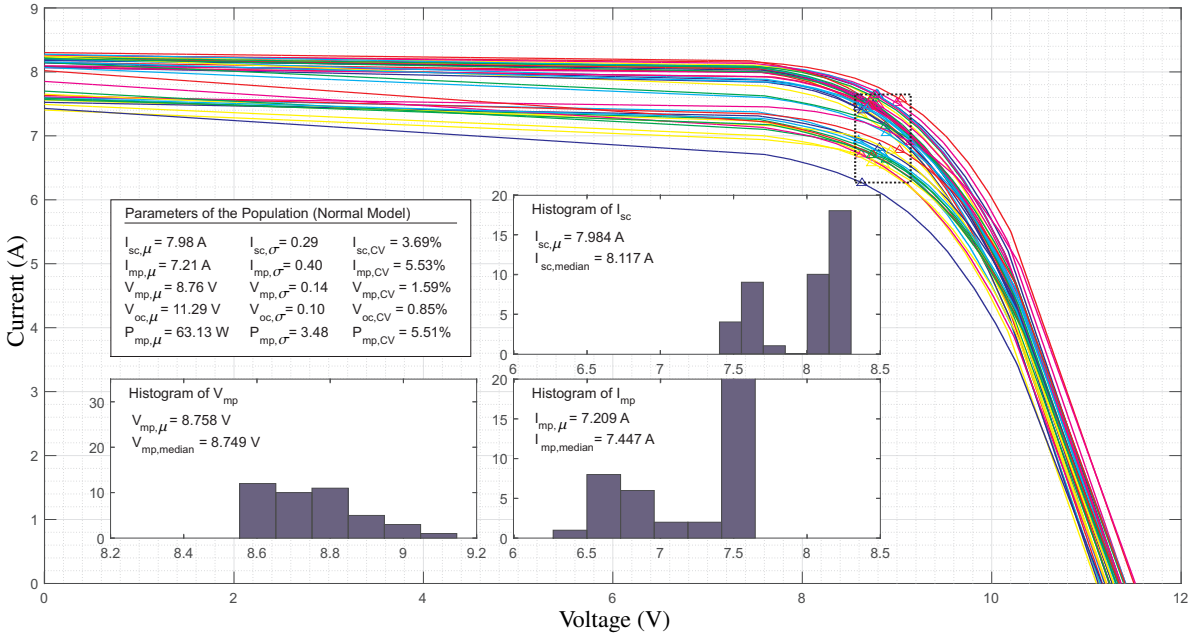

(b) Measurements in March 2019 (9 years old).

Figure 2: V-I Plot of the 42 submodules. The △ marks point to the MPP of the curves, which are within the limits of the dotted black box. Four boxes describe the statistical attributes of the curves. The top left box shows the average value, the standard deviation and the coefficient of variation of I_{sc}, I_{mp}, V_{mp}, V_{oc}, and P_{mp} of these 42 curves. The bottom left box shows the histogram of the 42 V_{mp} values, and compares average and median values. The top and bottom right boxes show the histograms of I_{sc} and I_{mp}.

with previous studies. However, the rate of increase of the CV of I_{sc} is 0.25-0.29% per year, a value slightly below the 0.36%/year reported at the module level in (Jordan et al., 2012). In contrast, the rate of increase of

Table 2: Statistical comparison of submodule parameters at NOCT: Year zero (from datasheet), 7 years old (from 42 measurements) and 8 years old (from 42 measurements).

Parameter	Year	I_{sc} (A)	I_{mp} (A)	V_{mp} (V)	V_{oc} (V)	P_{mp} (W)
Average μ	From Datasheet	8.68	7.94	8.77	11.3	69.58
	7 years old	8.14	7.36	8.80	11.27	64.8
	8 years old	8.08	7.32	8.76	11.28	64.16
	9 years old	7.98	7.21	8.76	11.29	63.13
μ Change/year	Datasheet v. 7 years	-0.89%	-1.04%	0.05%	0.04%	-0.98%
	Datasheet v. 8 years	-0.86%	-0.98%	-0.01%	-0.02%	-0.97%
	Datasheet v. 9 years	-0.88%	-1.01%	-0.01%	-0.01%	-1.02%
CV	From Datasheet	1%	1%	-	-	1%
	7 years old	2.76%	4.62%	1.36%	0.71%	4.37%
	8 years old	3.22%	4.92%	1.60%	0.89%	4.38%
	9 years old	3.69%	5.52%	1.59%	0.84%	5.51%
CV Change/year	Datasheet v. 7 years	0.25%	0.51%	-	-	0.48%
	Datasheet v. 8 years	0.27%	0.49%	-	-	0.42%
	Datasheet v. 9 years	0.29%	0.50%	-	-	0.50%

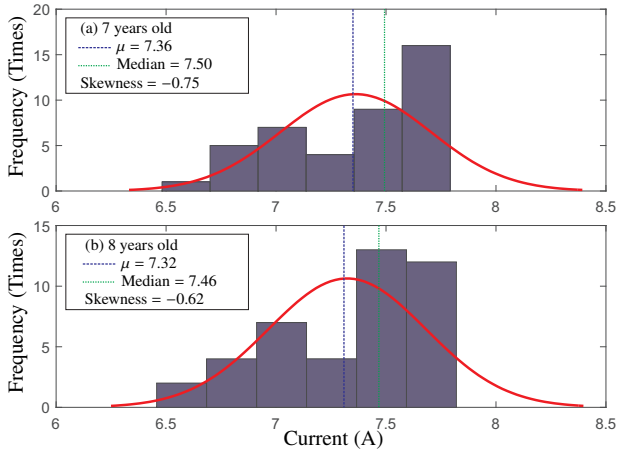

Figure 3: Histogram of the I_{mp} measurements (42 submodules): (a) when the system is 7 years old and (b) when the system is 8 years old. Red line: fitting of the measurements with a normal distribution. Blue dashed line: mean value. Green dotted line: median value.

the CV of I_{mp} is well above those values and corresponds to 0.49-0.51%/year. This last result demonstrates that the CV of I_{mp} is larger than that of I_{sc}. Also, it shows that previous module-level based predictions have underestimated the effects of ageing mismatch at the submodule-level.

It must be remarked that the degradation rates and the increase of the CVs is consistent throughout the three years of measurements, thus being in good agreement with the linearity of these effects with respect to time. Also, it has to be pointed out that the statistical analysis shown above considers that the probability density function that describes the set of measurements is normal. Nonetheless, as shown in Fig. 3, the difference between the mean and the median values of the maximum power point current indicates a non-normal distribution. The following subsection explores a probability density function model that includes skewness.

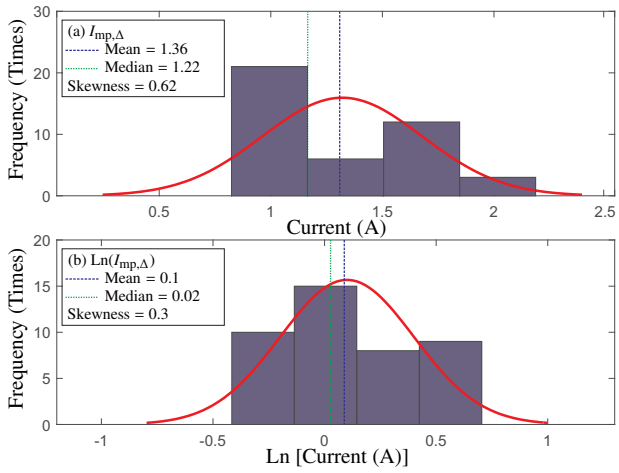

Figure 4: (a) Histogram of $I_{mp,\Delta} = 8.68 - I_{mp}$ when the system is 8 years old. (b) Histogram of the natural logarithm of $I_{mp,\Delta} = 8.68 - I_{mp}$ when the system is 8 years old. Red line: fitting of the histograms with a normal distribution. Blue dashed line: mean value. Green dotted line: median value.

3.2. Submodule Level Mismatch Modeling

This subsection presents a subexponential heavy-tailed distribution (Kotz, 1988) that can describe appropriately the properties of the measurements. Only the measurements of I_{mp} are considered, since the MPP current is the main parameter affecting the efficiency of the PV system. The results of Fig. 3 point to a negative skewness, which is in line with previous reports (Jordan et al., 2012). The distribution tends to include most of its contents within a small range around the median, whereas there is a decreasing chance of cases where the current is smaller. It is worth to point out that in our set of measurements, the histogram of I_{mp} shows an unexpected 'gap' near the median. This gap should typically not exist (Jordan and Kurtz, 2011), and other than that, the measurements are in good agreement with the literature.

One-tailed arrangements, including the Weibull, Burr or the log-normal distributions (Kotz, 1988), can be used to model such a probability density function (PDF). In that sense, the log-normal distribution presents the advantage that its relationship with the normal distribution can be used to characterize the PDF easily. Nonetheless, the log-normal distribution can only be used to represent positive skewness (i.e.: right-tailed distributions), while Fig. 3 shows negative skewness. In order to adapt the probability density function describing the MPP current to the positive skewness of the log-normal distribution, the following transformation is carried out. The measurements are subtracted from the short-circuit current specified in the datasheet.

$$I_{mp,\Delta} = 8.68 - I_{mp}. \tag{1}$$

Fig. 4(a) shows the new histogram of the 8-years old I_{mp} measurements after the transformation. Now the x-axis points to the decrease of the MPP current with respect to the datasheet short-circuit current. In addition, the appropriateness of the log-normal distribution can be observed in Fig. 4(b), where the histogram of natural logarithm of the measurements is depicted. If the log-normal distribution is pertinent, then the logarithm of the variable presents a normal distribution (Kotz, 1988). Although some level of skewness (which is related to the aforementioned lack of measurements near the median in this set) still exists, it can be seen that the normal distribution is in good agreement with the histogram.

The log-normal distribution is characterized by its mean and standard deviation, noted μ^*_Δ and σ^*_Δ respectively. These parameters can be easily related to μ_Δ and σ_Δ from the normal distribution as follows

Table 3: Predicted statistical parameters after 1, 7, 25 and 50 years.

Parameter	Year 1	Year 7	Year 25	Year 50
μ_Δ (A)	0.74	1.32	2.68	4.61
CV w.r.t. μ (%)	1	4.62	12.45	25.5
$\sigma = \sigma_\Delta$	0.0794	0.3435	0.7477	1.0367
μ^*_Δ	-0.3068	0.2432	0.9473	1.5047
σ^*_Δ	0.1070	0.2563	0.2740	0.2219

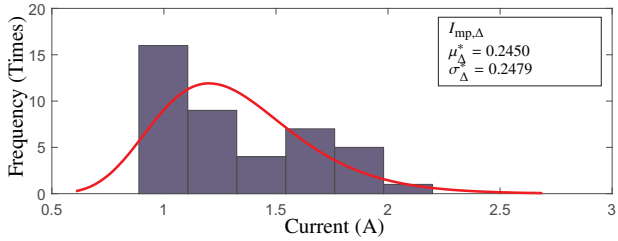

Figure 5: Histogram of $I_{mp,\Delta} = 8.68 - I_{mp}$ when the system is 7 years old. Red line: log-normal fitting of the measurements. The μ^*_Δ and σ^*_Δ parameters of the log-normal fitting agree with those in Table 3.

(Johnson et al., 1995):

$$\mu^*_\Delta = \ln\left(\frac{\mu^2_\Delta}{\sqrt{\sigma^2_\Delta + \mu^2_\Delta}}\right), \tag{2}$$

$$\sigma^*_\Delta = \sqrt{\ln\left(\frac{\sigma^2_\Delta}{\mu^2_\Delta} + 1\right)}. \tag{3}$$

Considering that the changes of the 8 and 9-years old μ and CV of I_{mp} in Table 2 are linear (such as in (Vázquez and Rey-Stolle, 2008)), the corresponding probability density function for $I_{mp,\Delta}$ after 1, 7, 25 and 50 years should present the parameters of Table 3. In the table, also the modified versions μ^*_Δ and σ^*_Δ for the proposed log-normal distribution are given. The parameters of the 7 years old distribution have been verified in Fig. 5, where the histogram of $I_{mp,\Delta}$ from the measurements and a fitting of the log-normal distribution has been carried out, using an equivalent maximum likelihood parameter estimation (Stedinger, 1980). It can be seen that the parameters from the fitting are in good agreement with those from equations (2) and (3) in Table 3.

It is worth noting that the coefficient of variation of a I_{mp} population depends on its average. Since the average is decreasing with time, the assumption of linear changes in the CV accounts for the deceleration of the widening of the population. The evolution of the $I_{mp,\Delta}$ model with time has been depicted in Fig. 6.

4. Prediction of performance loss due to ageing submodule-level mismatch

The model presented in the previous section has been employed in a simulation of 25 years of life of the PV system under test. The objective of the simulation is not to predict the effect of the measured degradation, which is in good agreement with the literature, but to predict the effect of the newly measured submodule-level mismatch, with respect to previous module-level results. In order to decouple degradation

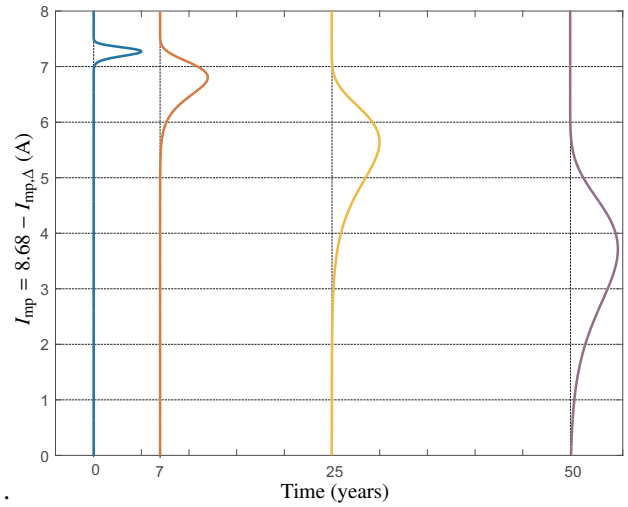

Figure 6: Log-normal distributions of I_{mp} when the system is new and when it is 7, 25, and 50 years old.

and mismatch loss, the simulation considers the energy obtained in a conventional series connection of the modules with respect to the maximum available energy if all submodules could operate at their corresponding maximum power points.

Since the simulation depends on the statistical model developed above, a Monte Carlo approach is used, such that 100 populations (or sets) of I_{mp} following the statistical model proposed above are generated. The parameters of the statistical model are those given in Table 3. The PV system under test is simulated first, hence the sets consist of 42 different submodule I_{mp}. Then, simulations of PV systems with 48 and 21 submodules in series are shown in Section 4.1. The populations are simulated using the tool described in (Olalla et al., 2013) and the average value of the outputs is taken as the expected value (Olalla et al., 2015).

Before assessing the impact of submodule mismatch on the energy yield and the efficiency of the system, the first result compares the generation of random populations following the normal model (as used in the past) and following the newly proposed log-normal model. The average and standard deviation of year 1 and year 25, as specified in Table 3, have been used. The results can be seen in Fig. 7. Given that the newly measured increase of the CV is larger than before, considering a normal population causes problems in the generation of a realistic population. In the figure, it can be seen how the normal model introduces unfeasible cases where the current increases with age (Fig 7(a)). This problem had been already detected in (Olalla et al., 2015) (with a lower chance of incidence, due to smaller CV values), where it was solved by generating as many populations as necessary until such a condition was not detected. Fig. 7(b) shows one possible result of that policy. Although the currents are always decreasing, it can be observed how some cases are still unrealistic and present nearly no dependence on time. The proposed log-normal model does not present this problem and it does not require the detection of the unrealistic cases (Fig. 7(c)).

Also the effect of the model can be seen in Fig. 8 where the efficiency of the system with the normal and the log-normal models is compared. Although the final value of efficiency is very similar in both cases (around 87%), the shape of the curve with the proposed log-normal model exhibits a larger loss since the early stage of ageing, which results in larger energy yield penalties. In this specific case, the lifetime recoverable loss with the normal model is 4.83%, whereas it increases up to 5.58% with the log-normal approach.

More importantly, Fig. 9(a) shows the comparison between the models with module-level data from (Jordan et al., 2012) and the newly reported submodule-level measurements. In order to maintain the

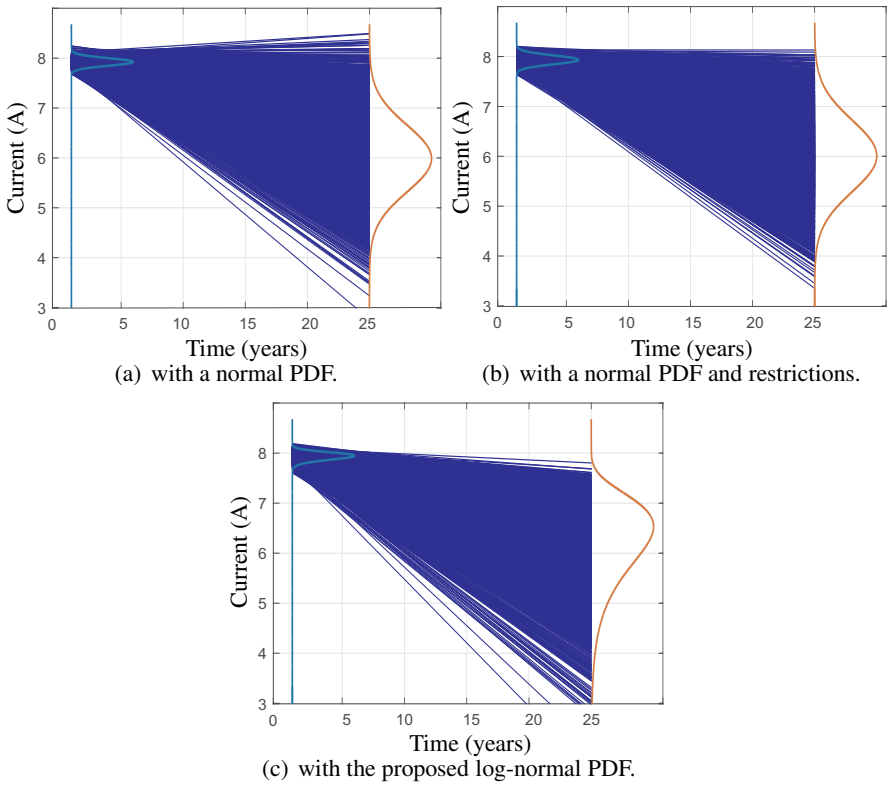

(a) with a normal PDF.
(b) with a normal PDF and restrictions.
(c) with the proposed log-normal PDF.

Figure 7: Example of evolution of I_{mp} in 25 years.

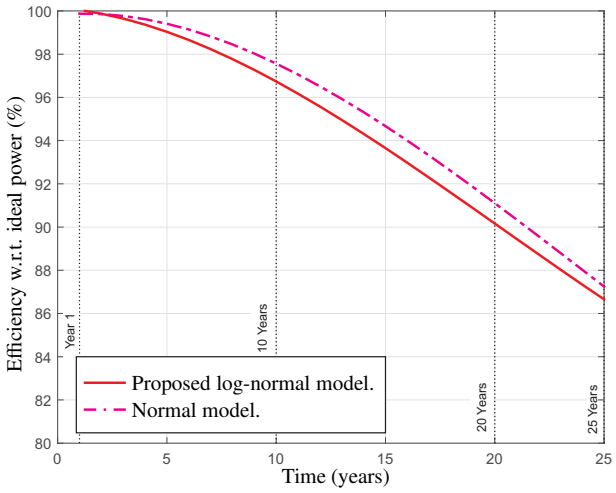

Figure 8: Efficiency of the system with respect to the ideal power: using the reported submodule-level measurements and the proposed log-normal model (solid line) and using the submodule-level measurements and a normal model (dash-dotted line).

comparison in good agreement with the data in (Jordan et al., 2012), the module-level models consider a degradation of -0.6% and an increase of the CV of +0.36% of the maximum power point current. In the figure, it can be seen that the submodule-level efficiency curve is the same shown in Fig. 8 and exhibits a 87% efficiency after 25 years. In contrast the module-level curve predicts a remarkably higher efficiency of

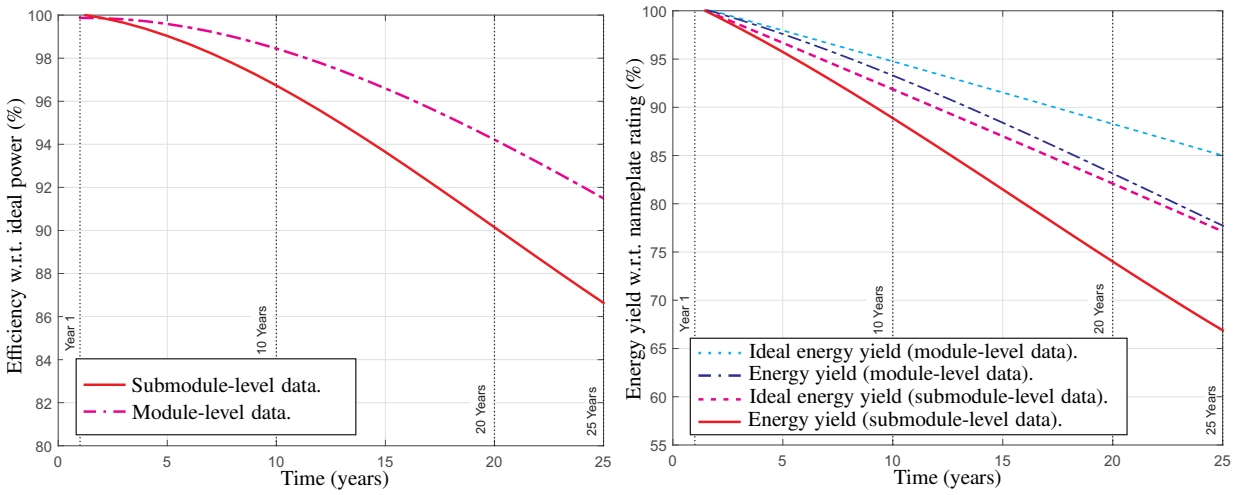

(a) Efficiency and time.

(b) Energy yield and time.

Figure 9: Comparison between module and submodule-level models. (a) Efficiency of the system with respect to the ideal power with submodule-level measurements (solid line) and using module level measurements from (Jordan et al., 2012) with a normal model (dash-dotted line). (b) Energy yield of the system with respect to the nameplate rating if all submodules could operate in their corresponding MPP, with module-level data (dotted line) and submodule-level data (dashed line). Energy yield of the system with respect to the nameplate rating in a conventional series connection, with module-level data (dash-dotted line) and submodule-level data (solid line).

Table 4: Simulation Results: Efficiency and Energy Loss

	Module-Level Data from (Olalla et al., 2015)	Novel Submodule-Level Data
Last Year Efficiency (%)	91.5%	**87%**
Total Lifetime Loss (%)	3.17%	**5.58%**

about 91.5%.

The effect of such differences can be seen in Fig. 9(b), where the energy yield in both cases is compared. The figure shows the ideal and the actual energy yield (with respect to nameplate rating) in case of a conventional series connection of the modules, again with the module-level data from (Jordan et al., 2012). The lifetime recoverable loss in that case is 3.17%, in good agreement with the recoverable energy predicted for a similar system in (Olalla et al., 2015). In comparison with module-level data, the submodule-level simulations reveal two main points. The data presented in the paper predict a 1% yearly degradation, hence the steeper decline of the energy yield. More significantly, the predicted lifetime energy loss accounts for 5.58%, which represents an increase of 76% with respect to the 3.17% predicted above. A summary of the different predictions can be seen in Table 4.

4.1. Comparison with Previously Reported Predictions

Finally, this subsection presents novel predictions for the two scenarios that were reported in (Olalla et al., 2015). The new submodule-level data introduce larger dispersion in the maximum power point currents, such that the newly obtained results exhibit a larger coefficient of recoverable energy.

Fig. 10(a) shows the efficiency of a utility-scale system (referred to as Scenario IV in (Olalla et al., 2015). The module-level data predicted an efficiency loss of about 7% after 25 years, which resulted in an

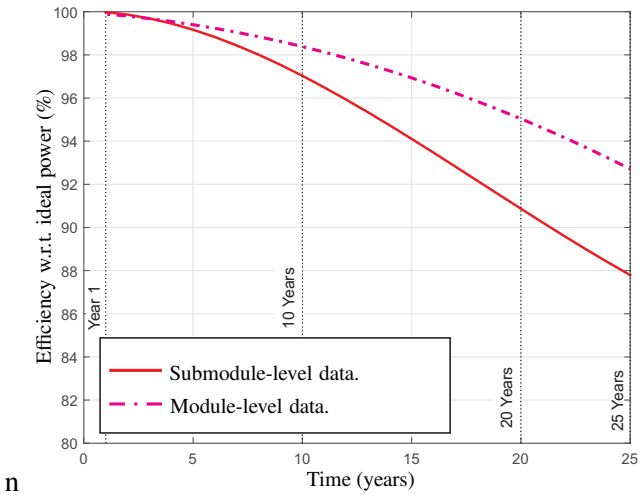

(a) Efficiency and time.

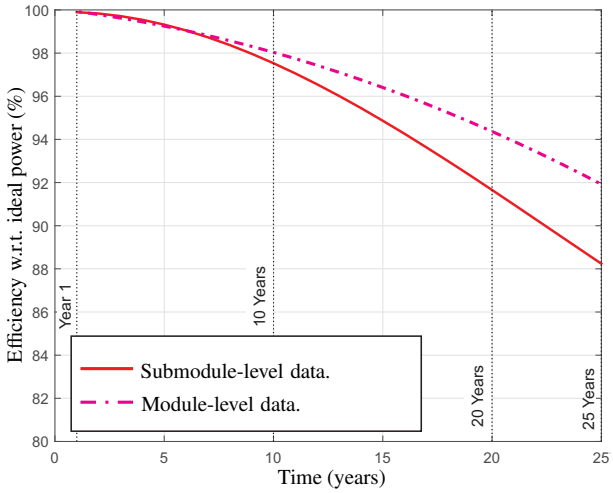

(b) Efficiency and time.

Figure 10: Comparison between the results with module-level data in (Olalla et al., 2015) and the results with new submodule-level models. (a) Utility scale system (Scenario IV in (Olalla et al., 2015)). (b) Residential system (Scenario V in (Olalla et al., 2015)).

overall lifetime loss of 2.74%. The novel submodule-level data show that the recoverable loss in year 25 increases up to 12 %, whereas the overall lifetime loss is twice as large as before, nearly 5%.

Similarly, Fig. 10(b) shows the efficiency of a residential system (referred to as Scenario V in (Olalla et al., 2015). The module-level data yielded last year and lifetime losses of 8.2% and 3.26%, respectively. The submodule-level model provides much the same results of the previous case, with a 25 years loss of 12% and a lifetime loss of 4.55%.

The prior module-level predictions and the novel results can be inspected in Table 5. In summary, the novel data predict that the recoverable loss after 25 years of operation does not depend heavily on the number of PV modules in series and it is close to 5%. This number nearly doubles the previous predictions, with a 75% and 80% increase in each case.

Table 5: Lifetime Energy Loss in Representative Systems

	Module-Level Data from (Olalla et al., 2015)	Novel Submodule Level Data
Recoverable Energy Loss Utility-Scale System (%)	2.74%	4.99%
Recoverable Energy Loss Residential System (%)	3.26%	4.55%

4.2. Discussion of the Results

The model presented in this paper is based on a 8 years old poly-Si PV system. Although the measurements throughout years 7, 8 and 9 show reasonable correlation, the data have been extrapolated in order to predict the CV of the system after 25 years. In this sense, the predictions must be validated in the future.

Nonetheless, the models show that the recoverable energy loss due to ageing may have been underestimated in the past. In absence of partial shading or any other source of mismatch, the recoverable loss during 25 years of operation of a PV system is between 4 and 6%. These quantities may offer an opportunity for submodule-level power electronics converters that mitigate mismatch and provide nearly 100% recovery of the energy loss due to current mismatch (Olalla et al., 2017).

Considering a simplified version of the levelized cost of energy (LCOE) as defined below

$$\mathrm{LCOE} = \frac{\mathrm{Cost}}{\mathrm{Energy}}\ , \tag{4}$$

an increase of the energy yield Δ in the range of 4 - 6% results in an almost linear decrease of the LCOE:

$$\mathrm{LCOE}^{*} = \left.\frac{\mathrm{Cost}}{\mathrm{Energy}(1+\frac{\Delta}{100})}\right|_{\frac{\Delta}{100}\to 0} \approx \mathrm{LCOE}(1-\frac{\Delta}{100}). \tag{5}$$

In other words, the LCOE would decrease approximately 4 - 6%, if the energy could be recovered. Such improvement requires power electronic converters whose cost is below the reported 4 - 6% gain. Considering that the cost of PV systems has decreased steadily to less than 1 € per installed peak Watt since 2012 (Fraunhofer Institute for Solar Energy Systems, 2018), it is yet to be seen whether the cost of the converters can meet such a small margin. Although a cost analysis is out of the scope of the paper, a quantification on this particular subject was performed in the context of partial shading in (Choi, 2015).

5. Conclusions

PV systems based on series-connected PV cells are affected by ageing mismatches, which can result in power losses that are fully recoverable. The influence of this source of mismatch has been reported in the past, by means of simulations, showing that the recoverable energy yield in the 25 years lifetime of a PV system is approximately 3%. However, these predictions have used ageing models based on module-level measurements, since there are no reports showing the effects of ageing at higher granularities.

In its first part, this paper has presented a set of submodule-level measurements of a PV system after 7, 8 and 9 years of use. The measurements have shown good agreement with the literature in the degradation rates of the currents I_{sc} and I_{mp}, and also in the small coefficient of variation of voltages V_{oc} and V_{mp}. In addition, the new measurements show good agreement with the negative skewness of I_{sc} and I_{mp} in previously reported cases. However, the measured standard deviation or the equivalent CV at the submodule

level has shown remarkable differences. Although the reported short-circuit current CV is slightly below what has been reported in the literature at the module level, the measured CV of I_{mp} is significantly larger than previously reported values. In consequence, previous predictions on the recoverable power and energy may have underestimated the effects of this source of mismatch.

The second part of the paper has presented an assessment of the recoverable energy due to aging, using a novel log-normal PDF that takes into account the new results of the measurements and also the skewness of the population. The comparison between 25 years simulations of the PV system under test with the statistical data reported in the past and the new submodule-level data show a significant increase in the total recoverable energy loss. Although the module level models show a lifetime recoverable loss of 3%, the novel models show that the recoverable loss is approximately 75% higher, totalling a loss of 5.58%. These numbers have been further validated in representative PV system scenarios that were reported in the past: module-level models were shown to present a loss, throughout the lifetime of the system, of 2.5 - 3.5%, whereas the novel models predict a fully recoverable loss of approximately 5%.

References

Borri, C., Gagliardi, M., Paggi, M., 2018. Fatigue crack growth in silicon solar cells and hysteretic behaviour of busbars. Solar Energy Materials and Solar Cells 181, 21–29.

Chamberlin, C. E., Rocheleau, M. A., Marshall, M. W., Reis, A. M., Coleman, N. T., Lehman, P. A., 2011. Comparison of PV module performance before and after 11 and 20 years of field exposure. In: Proc. of the IEEE Photovoltaic Specialists Conference (PVSC). pp. 101–105.

Choi, B., 2015. Differential power processing submodule integrated converters for photovoltaic power systems. Ph.D. thesis, University of Colorado.

Fraunhofer Institute for Solar Energy Systems, 2018. Photovoltaics report. [Online] Available here: https://www.ise.fraunhofer.de/en/publications/studies/photovoltaics-report.html.

Gagliardi, M., Lenarda, P., Paggi, M., 2017. A reaction-diffusion formulation to simulate EVA polymer degradation in environmental and accelerated ageing conditions. Solar Energy Materials and Solar Cells 164, 93–106.

Gagliardi, M., Paggi, M., 2018. Long-term EVA degradation simulation: Climatic zones comparison and possible revision of accelerated tests. Solar Energy 159, 882–897.

Gagliardi, M., Paggi, M., 2019. Multiphysics analysis of backsheet blistering in photovoltaic modules. Solar Energy 183, 512–520.

IEC, 2006. Photovoltaic devices - part 1: Measurement of photovoltaic current-voltage characteristics. Tech. rep., IEC-60904-1.

IEC, 2009. Photovoltaic devices - procedures for temperature and irradiance corrections to measured I-V characteristics. Tech. rep., IEC-60891.

IEC, 2011. Photovoltaic devices - part 5: Determination of the equivalent cell temperature (ECT) of photovoltaic (PV) devices by the open-circuit voltage method. Tech. rep., IEC-60904-5.

Johnson, N. L., Kotz, S., Balakrishnan, N., 1995. Continuous univariate distributions. Wiley.

Jordan, D., Wohlgemuth, J., Kurtz, S., 2012. Technology and climate trends in PV module degradation. In: 27th European Photovoltaic Solar Energy Conference and Exhibition, PVSEC. Frankfurt, Germany, pp. 3118 – 3124.

Jordan, D. C., Kurtz, S. R., 2011. Photovoltaic degradation rates - an analytical review. Progress in Photovoltaics: Research and Applications 21 (1), 12–29.

Jordan, D. C., Kurtz, S. R., VanSant, K., Newmiller, J., 2016. Compendium of photovoltaic degradation rates. Progress in Photovoltaics: Research and Applications.

Kotz, S., 1988. Encyclopedia of statistical sciences.

Makrides, G., Zinsser, B., Schubert, M., Georghiou, G. E., 2014. Performance loss rate of twelve photovoltaic technologies under field conditions using statistical techniques. Solar Energy 103, 28–42.

Mikofski, M. A., Kavulak, D. F. J., Okawa, D., Shen, Y. C., Terao, A., Anderson, M., Caldwell, S., Kim, D., Boitnott, N., Castro, J., Smith, L. A. L., Lacerda, R., Benjamin, D., Hasselbrink, E. F., 2012. Pvlife: An integrated model for predicting pv performance degradation over 25+ years. In: IEEE Photovoltaic Specialists Conference. pp. 1744–1749.

Olalla, C., Clement, D., Maksimovic, D., Deline, C., 2013. A cell-level photovoltaic model for high-granularity simulations. In: Proc. of the IEEE European Conference on Power Electronics and Applications (EPE-ECCE).

Olalla, C., Deline, C., Clement, D., Levron, Y., Rodriguez, M., Maksimovic, D., 2015. Performance of power limited differential power processing architectures in mismatched PV systems. IEEE Transactions on Power Electronics 30 (2), 618–631.

Olalla, C., Maksimovic, D., Deline, C., Martinez-Salamero, L., 2017. Impact of distributed power electronics on the lifetime and reliability of pv systems. Progress in Photovoltaics: Research and Applications In press.

Polverini, D., Field, M., Dunlop, E., Zaaiman, W., 2013. Polycrystalline silicon PV modules performance and degradation over 20 years. Progress in Photovoltaics: Research and Applications 21 (5), 1004–1015.

Pozza, A., Sample, T., 2016. Crystalline silicon PV module degradation after 20 yars of field exposure studied by electrical tests, electroluminescence, and LBIC. Progress in Photovoltaics: Research and Applications 24 (3), 368–378.

Pulver, S., Cormode, D., Cronin, A., Jordan, D., Kurtz, S., Smith, R., 2010. Measuring degradation rates without irradiance data. In: IEEE Photovoltaic Specialists Conference. pp. 1271–1276.

Reis, A. M., Coleman, N. T., Marshall, M. W., Lehman, P. A., Chamberlin, C. E., 2002. Comparison of pv module performance before and after 11-years of field exposure. In: Conference Record of the Twenty-Ninth IEEE Photovoltaic Specialists Conference. pp. 1432–1435.

Stedinger, J. R., 1980. Fitting log normal distributions to hydrologic data. Water Resources Research 16 (3), 481–490.

Vázquez, M., Rey-Stolle, I., 2008. Photovoltaic module reliability model based on field degradation studies. Progress in Photovoltaics: Research and Applications 16 (5), 419–433.

Zoellick, J. I., 1990. Testing and matching photovoltaic modules to maximize solar electric array performance. Ph.D. thesis, Humboldt State University.